IEEE Access
Multidisciplinary | Rapid Review | Open Access Journal

Received January 7, 2021, accepted January 11, 2021, date of publication January 21, 2021, date of current version February 1, 2021.

Digital Object Identifier 10.1109/ACCESS.2021.3053323

Security at the Physical Layer Over GG Fading and mEGG Turbulence Induced RF-UOWC Mixed System

A. S. M. BADRUDDUZA[1,*], (Member, IEEE), MD. IBRAHIM[2,*], S. M. RIAZUL ISLAM[3,*], (Member, IEEE), MD. SHAKHAWAT HOSSEN[1], (Member, IEEE), MILTON KUMAR KUNDU[4], (Member, IEEE), IMRAN SHAFIQUE ANSARI[5], (Member, IEEE), AND HEEJUNG YU[6,7], (Senior Member, IEEE)

[1]Department of Electronics and Telecommunication Engineering, Rajshahi University of Engineering and Technology (RUET), Rajshahi 6204, Bangladesh
[2]Department of Electrical and Electronic Engineering, Rajshahi University of Engineering and Technology (RUET), Rajshahi 6204, Bangladesh
[3]Department of Computer Science and Engineering, Sejong University, Seoul 05006, South Korea
[4]Department of Electrical and Computer Engineering, Rajshahi University of Engineering and Technology (RUET), Rajshahi 6204, Bangladesh
[5]James Watt School of Engineering, University of Glasgow, Glasgow G12 8QQ, U.K.
[6]Department of Electronics and Information Engineering, Korea University, Sejong 30019, South Korea
[7]Interdisciplinary Graduate Program for Artificial Intelligence Smart Convergence Technology, Korea University, Sejong 30019, South Korea

Corresponding authors: Milton Kumar Kundu (milton.kundu@ece.ruet.ac.bd) and Heejung Yu (heejungyu@korea.ac.kr)

*A. S. M. Badrudduza, Md. Ibrahim, and S. M. Riazul Islam are co-first authors.

This work was supported in part by the National Research Foundation of Korea grant funded by the Korean Government (Ministry of Science and ICT) under Grant 2019R1A2C1083988, in part by the Ministry of Science and ICT, South Korea, under the Information Technology Research Center Support Program supervised by the Institute for Information and Communications Technology Planning and Evaluation, under Grant IITP-2021-2016-0-00313, and in part by Sejong University through its Faculty Research Program under Grant 20202021.

ABSTRACT With the rapid evolution of communication technologies, high-speed optical wireless applications under the water surface as a replacement or complementary to the conventional radio frequency (RF) and acoustic technologies are attracting significant attention from the researchers. Since underwater turbulence (UWT) is an inevitable impediment for a long distance underwater optical wireless communication (UOWC) link, mixed RF-UOWC is being considered as a more feasible solution by the research community. This article deals with the secrecy performance of a variable gain relay-based mixed dual-hop RF-UOWC framework under the intercepting attempt of a potential eavesdropper. The RF link undergoes Generalized Gamma (GG) fading distribution, whereas the UOWC link is subjected to mixture Exponential Generalized Gamma (mEGG) distribution. The eavesdropper is capable of wiretapping via a RF link that also experiences the GG fading. The secrecy analysis incorporates the derivations of closed-form expressions for strictly positive secrecy capacity, average secrecy capacity, and exact as well as lower bound of secrecy outage probability in terms of univariate and bivariate Meijer's G and Fox's H functions. Based on these expressions, impacts of heterodyne and intensity modulation/direct detection techniques along with weak, moderate, and severe UWT conditions due to air bubbles, temperature, and salinity gradients are quantified. To the best of authors' knowledge, the proposed model is the first of its kind that addresses the secrecy analysis of a temperature gradient RF-UOWC system along with air bubbles, as opposed to the existing models that considered thermally uniform scenarios only. Finally, the derived expressions are verified via Monte-Carlo simulations.

INDEX TERMS Eavesdropper, optical wireless communication, physical layer security, under water turbulence.

I. INTRODUCTION

A. BACKGROUND AND LITERATURE STUDY

Wireless communication beneath the water surface is being considered as a growing research opportunity in recent times. To date, different types of communication strategies have been explored for underwater communication (UWC) systems including acoustic communication (ACOMM) [1], electromagnetic communications [2], optical wireless communications [3], and laser communications [4], [5]. However, underwater optical wireless communication (UOWC) in the form of light beams generated by laser or LED devices has

The associate editor coordinating the review of this manuscript and approving it for publication was Rui Wang.

been proven to be the most promising medium due to its high capacity, inherent robust security, low latency, lower energy consumption, and resistance to water link impairments [6]. In recent times, climate catastrophe and risk screening, coastal security, natural resource exploration, autonomous underwater robotics research, development of military underwater vehicles [7] and many other opportunities are highly dependent on the UOWC technology.

A comparative study among radio frequency (RF), acoustic, and optical signals was performed as a medium of underwater communication in [7]. The research found that UOWC possesses the highest data rate but suffers from absorption as well as scattering. The air-bubbles and temperature gradient in oceanic water create underwater turbulence (UWT) that was addressed in [8] using on-off keying (OOK) modulation scheme with spatial diversity under the assumption of log-normal distribution. The dispersion in different types of water, based on salinity, and transmission distance between various links in UOWC were analyzed in [9] using the OOK modulation, where the authors showed that the inter symbol interference is absent in the case of moderate turbulence in the seawater. A code-division multiple access (CDMA) based UOWC channel was proposed in [10] along with its possible design issues, architecture of the backhaul network, and associated network infrastructure. The effect of the bubbles size was experimented in [11]; the authors concluded that larger bubbles cause worse performance in UOWC as they block the optical light beams to pass through them. In [12], the authors performed a comparison between photo-multiplier tube and silicon photo-multipliers considering the span of the link along with the implementation problems of photo-multipliers from practical viewpoint. The capacity and symbol error rate of a UOWC channel were analyzed in [13] considering the UWT only.

Mixture exponential-Gamma (mEG) distribution was considered in [14] to analyze the effect of air bubbles in both salty and fresh waters and this model showed a perfect match with the experimented data. High speed data transfer is a prerequisite in state-of-the-art communication systems. In this regard, the authors in [15] performed an experiment to measure the data transfer rate in UOWC and a very high data rate was achieved at a distance of tens of meters. High speed data transfer was also attained in [16] using a specific blue LED with orthogonal frequency-division multiplexing (OFDM) technique. A method for non-line-of-sight communication through UOWC channel was proposed in [17] using back reflection technology that can be used to establish energy-efficient point to multipoint communications. A multihop UOWC system was described in [18] considering the effect of UWT and scattering in log-normal fading.

Different characteristics of the underwater scattering can be unified by the radiative transfer theory implemented in [19]. The work investigated the performance of UOWC taking the polarization behavior of light into account under varying distance. In [20], the authors evaluated the scintillation index of both spherical and plane light waves through a UOWC system with weak turbulence. A Weibull channel was proposed for UOWC in [21] to examine the effect of UWT for different salinity of water. The Generalized Gamma (GG) fading model-based UOWC was analyzed in [22] considering the UWT due to weak temperature gradient. Multi pulse-position modulation (PPM) technique was employed in [23] to study the performance of a UOWC system over log-normal distribution. The study demonstrated that multiple transmitting and receiving apertures-enabled spatial diversity is advantageous for capacity enhancement.

The advantages of the integration of underwater acoustic and optical channel that offers high speed data transfer at longer ranges were thoroughly described in [24]. The adverse effect of UWT along with general scattering and absorption was studied in [25] with receiving aperture diversity to increase the communication range. A new model using mixture exponential-generalized Gamma (mEGG) distribution was analyzed in [26] where the authors evaluated the system performances in terms of outage probability (OP), average bit error rate (ABER), and ergodic capacity (EC).

Although UOWC is the most promising technique for high speed underwater data transfer, the pressure and temperature-induced turbulence, due to some common phenomena (e.g. ocean currents) in the marine medium, leads to the degradation of the system performance [3], [27]. On that, researchers are paying attention to the development of a dual-hop RF-UOWC system [28]; the first hop communication occurs above the water surface using RF technology, whereas the second hop uses an UOWC connection to serve the coverage of interest under the water surface. These two communication mediums are linked through a relay that performs the required conversion of the RF signal into optical one for underwater transmission. A decode-and-forward (DF)-based mixed RF-UOWC system was introduced in [29] where the authors proposed Nakagami-m fading channel for the RF link and EGG distribution for the UOWC link. The RF channel was generalized with $\alpha - \mu$ distribution along with EGG model in [30]. In [31], a combination of Rayleigh and mEGG distributions was presented with both amplify-and-forward (AF) and DF relaying techniques, where the authors demonstrated that the complete system performance is affected by both the RF and UOWC links. An extension of this work was demonstrated in [32] considering Nakagami-m fading channel in the RF link.

Due to the rapid evolution of wireless networks, security concerns are drawing substantial attention from the researchers. Conventional security approaches follow cryptographic encryption methods at higher layers that are difficult to implement due to the complexity in secret key management. The physical layer security (PLS) approach is therefore emerging as one of the most effective ways of secure communications [33]–[35]. Note that the PLS utilizes the random attributes of the wireless channels to enhance the secrecy level instead of using any encryption key. Recently, secrecy analysis of a RF-UOWC link was investigated in terms of

intercept probability (IP) under eavesdropper's attack via a RF link [36]. A similar analysis was performed in [37], where the selection combining technique was employed at the relay's receiving node. The authors analyzed secrecy outage probability (SOP) and showed that SOP at high SNR regime is mostly dominated by UOWC path compared to RF link. Average secrecy capacity (ASC) and IP expressions were derived in [28] to depict the effects of a set of RF-UOWC system parameters on the secrecy capacity. To do so, the authors considered multi-antenna relay that utilizes maximal-ratio combining technique to recombine the received signals.

B. MOTIVATION AND CONTRIBUTIONS

Whereas the aforementioned studies show a comprehensive analysis of UOWC channels, only a few works mentioned the PLS in this domain. The researches in [28], [36], [37] analyzed the PLS over mixture exponential Gamma UOWC channel which is actually a special case of the mEGG model. The mEGG model is the most precise model to capture all the physical variations that can practically occur such as UWT, air bubbles, temperature change, and change in water salinity [26]. On the other hand, GG fading model comes with a couple of desirable advantages as the RF link. The versatility and mathematical tractability have made this channel very popular among the researchers. This general model comprises of some well-known multipath fading models such as Nakagami-m, Weibull, lognormal, and Rayleigh [38]. As only few works in the literature addressed the secrecy issues of RF-UOWC networks, the implementation of generalized fading and turbulence scenarios in both the RF and UOWC links is still an open area of investigation. As such, we in this paper propose a RF-UOWC mixed network; whereas the RF communication link undergoes GG distribution, the UOWC link experiences mEGG distribution. A relay node, placed between the source and the user, first receives RF signals from the source, converts the signal to an optical form, and finally forwards the signal to the intended user via the UOWC link. This transmission is carried out under the presence of an eavesdropper that tries to overhear the transmitted data via the same RF link. The major contributions of this work are highlighted as follows:

1. We derive the novel cumulative distribution function (CDF) of signal-to-noise ratio's (SNR)s for the mixed RF-UOWC scenario by utilizing the probability density function (PDF) of SNRs of each individual hop. The reason behind the novelty of demonstrated CDF is that the GG fading channel in combination with the mEGG distribution to form a mixed RF-UOWC system model is not noticed yet in the existing open literature. Moreover, Nakagami-m-mEGG [31], Nakagami-m-mEG [28], [37], and Nakagami-m-EGG [29] can be demonstrated as special cases of the proposed RF-UOWC model.
2. We analyze the secrecy performance of the dual-hop DF relaying systems via developing the expressions for ASC, exact and lower bound of SOP, and strictly positive secrecy capacity (SPSC) in terms of Meijer's G and Fox's H functions. These analytical expressions are unique and generalized in the sense that the considered dual-hop PDF and CDF for the proposed RF-UOWC system are unique and generalized, according to the authors' knowledge based on the open literature.
3. We demonstrate various numerical results based on the derived performance metrics that are further validated through Monte-Carlo (MC) simulations. In all cases, a strong agreement is found between the numerical and simulation results.
4. In evaluating the secrecy performances, we consider the impacts of air bubbles, salinity, and temperature gradient of the water and fading of RF links. Whereas the past comprehensive secrecy analyses considered only thermally uniform UOWC, the proposed UWT includes the impact of air bubbles for both types of scenarios (i.e. thermally uniform and temperature gradient), simultaneously present in fresh and salty water environment.
5. Moreover, we perform a comparative study between the two detection techniques i.e. heterodyne detection (HD) and intensity modulation/direct detection (IM/DD) and observe that the HD technique shows a better performance compared to IM/DD technique.

C. ORGANIZATION

Subsequent parts of this paper are organized as follows. Our proposed RF-UOWC system model is presented in Section II. Closed-form expressions of the performance metrics i.e. ASC, exact and lower bound of SOP and SPSC are derived in Section III. Whereas Section IV discusses the numerical and simulation results, Section V presents the summary of the work.

II. SYSTEM MODEL AND PROBLEM FORMULATION

The proposed dual-hop RF-UOWC system, comprised of a source node (S), a relay node (R), and a destination node (U), is presented in Fig.1. We assume U is located under the water surface. This specific form of communication scenario is getting immense popularity because of its recent utilization in oceanographic surveillance, offshore oil field exploration, unmanned undersea vehicles (UUV) research, coastal monitoring, and several military applications [27], [31]. The confidential communication between S and U via R is imperiled due to the presence of an undesirable eavesdropper (E) that thieves information using $S-E$ link. This model focuses on how the confidential signal from S can be safely transmitted to U via R defending against E. We assume S and E are equipped with a single antenna. In line with that, R has a single receive antenna and a single transmit aperture, and U has a single receive aperture.

Hence, in the proposed scenario, transmission of information is completed in two hops. The first hop is a surface

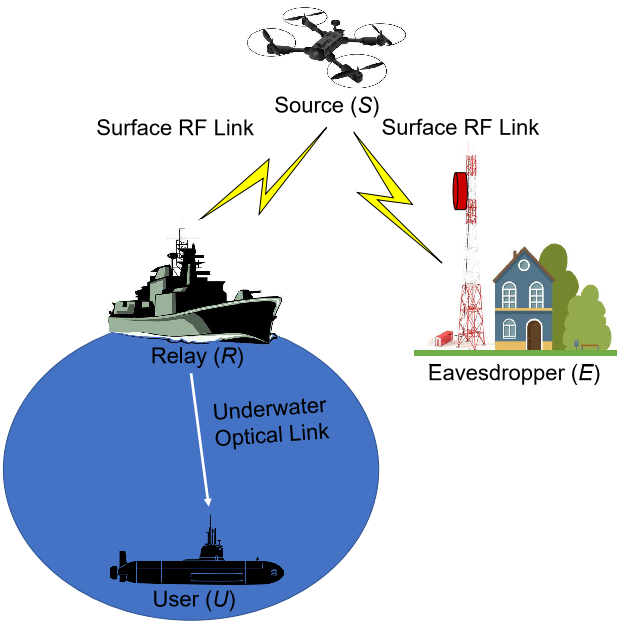

FIGURE 1. System model incorporating a source (*S*), a relay (*R*), an eavesdropper (*E*), and a desired user (*U*).

network wherein S transmits signal via $S-R$ RF path to R. The relay is capable of transforming received RF signal to its optical version and re-transmitting it to U via $R-U$ UOWC link. Therefore, the second hop is termed the underwater network. We consider E that utilizes the RF $(S-E)$ link for wiretapping. The surface RF communications experience GG fading distribution and the UOWC undergoes mEGG distribution.

Denoting the channel gains of $S-R$, $S-E$, and $R-U$ links as $a_{s,r} \in \mathbb{C}^{1\times 1}$, $b_{s,e} \in \mathbb{C}^{1\times 1}$, and $c_{r,u} \in \mathbb{C}^{1\times 1}$, respectively, we obtain the expression of received signals at R, E, and U as

$$y_{s,r} = a_{s,r}p + z_r, \tag{1a}$$
$$y_{s,e} = b_{s,e}p + z_e, \tag{1b}$$
$$\begin{aligned} y_{r,u} &= c_{r,u}y_{s,r} + z_u \\ &= c_{r,u}(a_{s,r}p + z_r) + z_u \\ &= d_{r,u}p + w_u. \end{aligned} \tag{1c}$$

Here, $p \sim \widetilde{\mathcal{N}}(0, P_s)$ is denoted as the transmitted RF signal from S, $d_{r,u} \triangleq c_{r,u}a_{s,r}$ is the channel gain of dual-hop $S-R-U$ link, $w_u \triangleq c_{r,u}z_r + z_u$, $z_r \sim \widetilde{\mathcal{N}}(0, N_r)$ and $z_e \sim \widetilde{\mathcal{N}}(0, N_e)$ are the RF noises at R and E, respectively, $z_u \sim \widetilde{\mathcal{N}}(0, N_u)$ stands for the imposed optical noise at U, N_r, N_e, and N_u are the corresponding noise powers, respectively and P_s represents transmit signal power. Note that the gain in the relay operation is included in the link gain of $c_{r,u}$. This gain can be regarded as η.

A. SNR OF EACH LINK

We denote the SNRs of $S-R$, $R-U$, and $S-E$ links as γ_R, γ_U, and γ_E, respectively, which are mathematically expressed as

$$\gamma_R = \frac{P_s}{N_r}\|a_{s,r}\|^2, \tag{2a}$$
$$\gamma_U = \frac{P_r}{N_u}\|c_{r,u}\|^2, \tag{2b}$$
$$\gamma_E = \frac{P_s}{N_e}\|b_{s,e}\|^2. \tag{2c}$$

Here, P_r is the transmit optical power from R. The received SNR of the combined RF-UOWC channel is given as [39, Eq. (5)]

$$\gamma_{eq} = \frac{\gamma_R\gamma_U}{\gamma_R+\gamma_U+1} \cong min\{\gamma_R, \gamma_U\}. \tag{3}$$

TABLE 1. Special cases of GG distribution [42], [43].

Envelope Distribution	a_R	C_R
Rayleigh	2	1
Nakagami-m	2	-
Weibull	-	1
Gamma	1	-
Exponential	1	1
Additive White Gaussian Noise (AWGN)	2	∞

B. PDF AND CDF OF γ_R

The PDF of γ_R follows the GG distribution as [40, Eq. (2)]

$$f_{\gamma_R}(\gamma) = K_1\gamma^{K_2}e^{-K_3\gamma^{\breve{a}}}, \tag{4}$$

where $K_1 = \frac{\breve{a}\,C_R^{C_R}}{\phi_R^{\breve{a}C_R}\Gamma(C_R)}$, $K_2 = \breve{a}\,C_R - 1$, $K_3 = C_R\,\phi_R^{-\breve{a}}$, $\breve{a} = \frac{a_R}{2}$, a_R is the fading parameter, ϕ_R indicates the average SNR of $S-R$ link, $\Gamma(.)$ denotes the Gamma operator, and C_R is termed as normalized variance parameter of GG fading model envelopes. Now, the CDF of γ_R is defined as

$$F_{\gamma_R}(\gamma) = \int_0^{\gamma} f_{\gamma_R}(\gamma)d\gamma. \tag{5}$$

By replacing (4) into (5) and utilizing [41, Eq. (3.381.8)], $F_{\gamma_R}(\gamma)$ is expressed as [40, Eq. (3)]

$$F_{\gamma_R}(\gamma) = \frac{\Upsilon(C_R, K_3\,\gamma^{\breve{a}})}{\Gamma(C_R)}, \tag{6}$$

where $\Upsilon(b,k) = \int_0^k e^{-z}z^{b-1}dz$ is a lower incomplete Gamma function [41, Eq. (8.350.1)]. Utilizing the identity from [41, Eq. (8.352.6)], (6) can be finally rewritten as

$$F_{\gamma_R}(\gamma) = 1 - e^{-K_3\,\gamma^{\breve{a}}}\sum_{q_1=0}^{C_R-1}\frac{K_3^{q_1}\gamma^{\breve{a}q_1}}{q_1!}. \tag{7}$$

It is clear from (7) that C_R is an integer. We assume that the proposed RF channel undergoes GG distribution as it provides immense flexibility to obtain some other recognized fading channels [42]–[44] as its special scenarios that are given in Table 1.

TABLE 2. EGG distribution parameters corresponding to temperature gradient UOWC link. [26].

Bubbles Level h (L/min)	Temperature Gradient l (C cm^{-1})	ω	λ	a	b	c
2.4	0.05	0.2130	0.3291	1.4299	1.1817	17.1984
2.4	0.10	0.2108	0.2694	0.6020	1.2795	21.1611
2.4	0.15	0.1807	0.1641	0.2334	1.4201	22.5924
2.4	0.20	0.1665	0.1207	0.1559	1.5216	22.8754
4.7	0.05	0.4589	0.3449	1.0421	1.5708	35.9484
4.7	0.10	0.4539	0.2744	0.3008	1.7053	54.1422
16.5	0.22	0.6238	0.1094	0.0111	4.4750	105.3550
23.6	0.22	0.7210	0.1479	0.0121	7.4189	65.6983

TABLE 3. EGG distribution parameters corresponding to thermally uniform UOWC link. [26].

Water Salinity	Bubbles Level h (L/min)	ω	λ	a	b	c
Salty Water	0	1.4684×10^{-23}	0.9853	1.0126×10^{3}	0.0344	2.0541
	2.4	0.1770	0.4687	0.7736	1.1372	49.1773
	4.7	0.2064	0.3953	0.5307	1.2154	35.7368
	7.1	0.4344	0.4747	0.3935	1.4506	77.0245
	16.5	0.4951	0.1368	0.0161	3.2033	82.1030
Fresh Water	0	4.0628×10^{-21}	1.0225	30.8432	0.6993	9.5461
	2.4	0.1953	0.5273	3.7291	1.0721	30.3214
	4.7	0.2109	0.4603	1.2526	1.1501	41.3258
	7.1	0.3489	0.4771	0.4319	1.4531	74.3650
	16.5	0.5117	0.1602	0.0075	2.9963	216.8356

C. PDF AND CDF OF γ_U

The UOWC link is subjected to mEGG distribution in the presence of UWT. Assuming both HD and IM/DD techniques, the PDF of γ_U is written as [26]

$$f_{\gamma_U}(\gamma) = \sum_{i=1}^{2} \mathcal{T}_i \gamma^{-1} G_{0,1}^{1,0}\left[\mathcal{Q}_i \gamma^{\mathcal{R}_i} \middle| \begin{matrix} - \\ \mathcal{S}_i \end{matrix}\right], \tag{8}$$

where $\mathcal{Q}_1 = \frac{1}{\lambda\, \mu_r^{\frac{1}{r}}}$, $\mathcal{R}_1 = \frac{1}{r}$, $\mathcal{S}_1 = 1$, $\mathcal{T}_1 = \frac{\omega}{r}$, $\mathcal{Q}_2 = \frac{1}{b^c \mu_r^{\frac{c}{r}}}$, $\mathcal{R}_2 = \frac{c}{r}$, $\mathcal{S}_2 = a$, $\mathcal{T}_2 = \frac{c(1-\omega)}{r\Gamma(a)}$, λ denotes the exponential distribution parameter, ω symbolizes the mixture weight, where $0 < \omega < 1$, a, b, and c stand for the GG distribution parameters, and $G_{p,q}^{m,n}[.]$ is the Meijer's G function as explained in [41]. For a special case with $c = 1$, (8) can be transformed to the PDF of exponential Gamma (EG) model [45]. Here, r indicates the detection technique (i.e. $r = 1$ denotes the HD technique and $r = 2$ represents the IM/DD technique), ϕ_U signifies the average SNR of UOWC link, where $\mu_1 = \phi_U$ and $\mu_2 = \frac{\phi_U}{2\,\omega\,\lambda^2 + b^2(1-\omega)\frac{\Gamma(a+\frac{2}{c})}{\Gamma(a)}}$ specifies the electrical SNR for HD and IM/DD techniques, respectively.

The values of ω, λ, a, b, and c were experimentally obtained in [26] considering various bubble levels and temperature gradients that correspond to different turbulence conditions (weak to strong) (Table 2) and for fresh and salty waters (Table 3). In Table 2, it is clearly noted that a certain increase in air bubbles level along with temperature gradient gradually generates weak, moderate, and strong turbulence conditions that helps us to determine the performance accuracy of proposed mEGG channel in the presence of turbulence induced fading conditions along with irradiance fluctuations in UOWC links. Table 3 also presents various turbulence scenarios that correspond to several air bubbles level in both fresh and salty water environment considering a thermally uniform UOWC network. Hence, performance of both UOWC systems (i.e. temperature gradient and thermally uniform) can be easily demonstrated utilizing mEGG model operating under a variety of turbulence conditions that makes this channel very much popular among the researchers.

Similar to (5), the CDF for UOWC link is obtained as [26]

$$F_{\gamma_U}(\gamma) = \sum_{i=1}^{2} \mathcal{P}_i G_{1,2}^{1,1}\left[\mathcal{Q}_i \gamma^{\mathcal{R}_i} \middle| \begin{matrix} 1 \\ \mathcal{S}_i, 0 \end{matrix}\right], \tag{9}$$

where $\mathcal{P}_1 = \omega$ and $\mathcal{P}_2 = \frac{1-\omega}{\Gamma(a)}$.

D. PDF AND CDF OF γ_E

Assuming S-E link also follows GG distribution, similar to (4), the PDF and CDF of γ_E is written as [40, Eqs. (2 and 3)]

$$f_{\gamma_E}(\gamma) = M_1 \gamma^{M_2} e^{-M_3 \gamma^{\check{b}}}, \tag{10}$$

and

$$F_{\gamma_E}(\gamma) = 1 - e^{-M_3\, \gamma^{\check{b}}} \sum_{e_1=0}^{C_E-1} \frac{M_3^{e_1} \gamma^{\check{b} e_1}}{e_1!}, \tag{11}$$

respectively, where $M_1 = \frac{\breve{b}\, C_E^{C_E}}{\phi_E^{\breve{b} C_E}\, \Gamma(C_E)}$, $M_2 = \breve{b}\, C_E - 1$, $M_3 = C_E\, \phi_E^{-\breve{b}}$, $\breve{b} = \frac{b_E}{2}$, ϕ_E is the average SNR for the $S-E$ channel, b_E indicates the fading parameter, and C_E symbolizes the normalized variance.

E. CDF OF SNR FOR DUAL-HOP RF-UOWC LINK

The CDF of γ_{eq} is expressed as [46, Eq. (15)]

$$F_{\gamma_{eq}}(\gamma) = Pr\{min(\gamma_R, \gamma_U) < \gamma\} = F_{\gamma_R}(\gamma) + F_{\gamma_U}(\gamma) - F_{\gamma_R}(\gamma) F_{\gamma_U}(\gamma). \quad (12)$$

Now substituting (7) and (9) into (12) and after simplification via some mathematical manipulations, the CDF of γ_{eq} is obtained as

$$F_{\gamma_{eq}}(\gamma) = 1 - e^{-K_3 \gamma^{\breve{a}}} \sum_{q_1=0}^{C_R-1} \frac{K_3^{q_1} \gamma^{\breve{a} q_1}}{q_1!} \times \left(1 - \sum_{i=1}^{2} \mathcal{P}_i G_{1,2}^{1,1}\left[\mathcal{Q}_i \gamma^{\mathcal{R}_i} \middle| \begin{matrix} 1 \\ \mathcal{S}_i, 0 \end{matrix}\right]\right). \quad (13)$$

To the best of authors' knowledge based on the open literature, the derived CDF expression in (13) is novel as combination of GG and mEGG distributions to model a dual-hop RF-UOWC network is not reported in any existing work yet. Besides, since both GG and mEGG models represent generalized distributions, (13) is also generalized that leads to the unification of several existing models as special cases.

III. PERFORMANCE ANALYSIS

With a view to analyzing the secrecy behaviour, we utilize (10), (11), and (13) in this section to derive novel analytical expressions of ASC, exact and lower bound of SOP, and SPSC for the proposed RF-UOWC framework.

A. AVERAGE SECRECY CAPACITY ANALYSIS

ASC is widely used as a secrecy metric for evaluating the secrecy performance of a wiretapped wireless system, where an eavesdropper can hamper the secure transmission between transmitter and receiver. Mathematically, ASC is defined as [47, Eq. (15)]

$$ASC = \int_0^\infty \frac{F_{\gamma_E}(\gamma)}{1+\gamma} \left\{1 - F_{\gamma_{eq}}(\gamma)\right\} d\gamma. \quad (14)$$

By substituting (11) and (13) into (14), the ASC is derived as

$$ASC = \sum_{q_1=0}^{C_R-1} \frac{K_3^{q_1}}{q_1!} \left[\Im_1 - \sum_{i=1}^{2} \mathcal{P}_i \Im_2 - \sum_{e_1=0}^{C_E-1} \frac{M_3^{e_1}}{e_1!} \times \left(\Im_3 - \sum_{i=1}^{2} \mathcal{P}_i \Im_4\right)\right], \quad (15)$$

where $\Im_1$, $\Im_2$, $\Im_3$, and $\Im_4$ are the four integral terms derived as follows.

1) DERIVATION OF $\Im_1$

Utilizing the identities from [48, Eqs. (8.4.2.5) and (8.4.3.1)] to transform $\frac{1}{1+\gamma}$ and $e^{-K_3\gamma^{\breve{a}}}$ terms into Meijer's G functions and performing integration utilizing [48, Eq. (2.24.1.1)], $\Im_1$ is derived as

$$\Im_1 = \int_0^\infty \frac{\gamma^{\breve{a} q_1}}{1+\gamma} e^{-K_3 \gamma^{\breve{a}}} d\gamma = \int_0^\infty \gamma^{\breve{a} q_1} G_{1,1}^{1,1}\left[\gamma \middle| \begin{matrix} 0 \\ 0 \end{matrix}\right] \times G_{0,1}^{1,0}\left[K_3 \gamma^{\breve{a}} \middle| \begin{matrix} - \\ 0 \end{matrix}\right] d\gamma = \frac{1}{(2\pi)^{\breve{a}-1}} G_{\breve{a},1+\breve{a}}^{1+\breve{a},\breve{a}}\left[K_3 \middle| \begin{matrix} \vartheta_1 \\ 0, \vartheta_1 \end{matrix}\right], \quad (16)$$

where $\vartheta_1 = \Delta(\breve{a}, -\breve{a} q_1)$ that represents the following sequence: $\Delta(d, r) = \frac{r}{d}, \frac{r+1}{d}, \ldots, \frac{r+d-1}{d}$ as defined in [49, Eq. (22)].

2) DERIVATION OF $\Im_2$

Applying the integral identities of [48, Eqs. (8.4.2.5) and (8.4.3.1)], $\Im_2$ is derived as

$$\Im_2 = \int_0^\infty \frac{\gamma^{\breve{a} q_1}}{1+\gamma} e^{-K_3 \gamma^{\breve{a}}} G_{1,2}^{1,1}\left[\mathcal{Q}_i \gamma^{\mathcal{R}_i} \middle| \begin{matrix} 1 \\ \mathcal{S}_i, 0 \end{matrix}\right] d\gamma = \int_0^\infty \gamma^{\breve{a} q_1} G_{1,1}^{1,1}\left[\gamma \middle| \begin{matrix} 0 \\ 0 \end{matrix}\right] G_{0,1}^{1,0}\left[K_3 \gamma^{\breve{a}} \middle| \begin{matrix} - \\ 0 \end{matrix}\right] \times G_{1,2}^{1,1}\left[\mathcal{Q}_i \gamma^{\mathcal{R}_i} \middle| \begin{matrix} 1 \\ \mathcal{S}_i, 0 \end{matrix}\right] d\gamma. \quad (17)$$

Now converting all the Meijer's G functions into Fox's H functions based on [50, Eq. (6.2.8)] and performing integration with the help of [51, Eq. (2.3)] and [52, Eq. (3)], $\Im_2$ is written in an alternative form as

$$\Im_2 = \int_0^\infty \gamma^{\breve{a} q_1} H_{1,1}^{1,1}\left[\gamma \middle| \begin{matrix} (0,1) \\ (0,1) \end{matrix}\right] H_{0,1}^{1,0}\left[K_3 \gamma^{\breve{a}} \middle| \begin{matrix} - \\ (0,1) \end{matrix}\right] \times H_{1,2}^{1,1}\left[\mathcal{Q}_i \gamma^{\mathcal{R}_i} \middle| \begin{matrix} (1,1) \\ (\mathcal{S}_i, 1), (0,1) \end{matrix}\right] d\gamma = K_3^{-(\breve{a} q_1 + 1)} \times H_{1,0:1,1:1,1:1,2}^{1,0:1,1:1,1}\left[\begin{matrix} J_1 \\ J_2 \end{matrix} \middle| \begin{matrix} (0,1) \\ (0,1) \end{matrix} \middle| \begin{matrix} (1,1) \\ (\mathcal{S}_i, 1), (0,1) \end{matrix} \middle| J_3, J_4\right], \quad (18)$$

where $J_1 = (-\breve{a} q_1; 1, \mathcal{R}_i)$, $J_2 = (1; -)$, $J_3 = \frac{1}{K_3}$, $J_4 = \frac{\mathcal{Q}_i}{K_3^{\mathcal{R}_i}}$, $H_{p,q}^{m,n}[.]$ is the Fox's H function introduced in [53, Eq. (1.2)], and $H_{c_1,d_1:c_2,d_2:c_3,d_3}^{x_1,y_1:x_2,y_2:x_3,y_3}[.]$ is the extended generalized bivariate Fox's H function (EGBFHF) as explained in [53, Eq. (2.57)].

3) DERIVATION OF $\Im_3$

Utilizing the identities from $\Im_2$, $\Im_3$ is derived as

$$\Im_3 = \int_0^\infty \frac{\gamma^{\breve{b} e_1 + \breve{a} q_1}}{1+\gamma} e^{-M_3 \gamma^{\breve{b}}} e^{-K_3 \gamma^{\breve{a}}} d\gamma = \int_0^\infty \gamma^{\breve{b} e_1 + \breve{a} q_1} H_{0,1}^{1,0}\left[M_3 \gamma^{\breve{b}} \middle| \begin{matrix} - \\ (0,1) \end{matrix}\right] H_{1,1}^{1,1}\left[\gamma \middle| \begin{matrix} (0,1) \\ (0,1) \end{matrix}\right] \times H_{0,1}^{1,0}\left[K_3 \gamma^{\breve{a}} \middle| \begin{matrix} - \\ (0,1) \end{matrix}\right] d\gamma = M_3^{-(\breve{b} e_1 + \breve{a} q_1 + 1)} \times H_{1,0:1,1:1,0:0,1}^{1,0:1,1:1,0}\left[\begin{matrix} J_5 \\ J_2 \end{matrix} \middle| \begin{matrix} (0,1) \\ (0,1) \end{matrix} \middle| \begin{matrix} - \\ (0,1) \end{matrix} \middle| J_6, J_7\right], \quad (19)$$

where $J_5 = (-\breve{b} e_1 - \breve{a} q_1; 1, \breve{a})$, $J_6 = \frac{1}{M_3}$, and $J_7 = \frac{K_3}{M_3^{\breve{a}}}$.

4) DERIVATION OF $\Im_4$

Finally, the integral $\Im_4$ is written as

$$\Im_4 = \int_0^\infty \frac{\gamma^{\breve{b}e_1+\breve{a}q_1}}{1+\gamma} e^{-M_3\gamma^{\breve{b}}} e^{-K_3\gamma^{\breve{a}}} G_{1,2}^{1,1}\left[\mathcal{Q}_i\gamma^{\mathcal{R}_i}\middle| \begin{matrix}1\\ \mathcal{S}_i, 0\end{matrix}\right] d\gamma. \tag{20}$$

Note that there exists no mathematical identities to solve (20). But considering $b_E = a_R$, performing integration in (20) is possible in a similar way to $\Im_2$ which is given as follows

$$\begin{aligned}\Im_4 &= \int_0^\infty \frac{\gamma^{\breve{a}Z_1}}{1+\gamma} e^{-Z_2\gamma^{\breve{a}}} G_{1,2}^{1,1}\left[\mathcal{Q}_i\gamma^{\mathcal{R}_i}\middle| \begin{matrix}1\\ \mathcal{S}_i, 0\end{matrix}\right] d\gamma \\ &= \int_0^\infty \gamma^{\breve{a}Z_1} H_{1,1}^{1,1}\left[\gamma\middle| \begin{matrix}(0,1)\\ (0,1)\end{matrix}\right] H_{0,1}^{1,0}\left[Z_2\gamma^{\breve{a}}\middle| \begin{matrix}-\\ (0,1)\end{matrix}\right] \\ &\quad \times H_{1,2}^{1,1}\left[\mathcal{Q}_i\gamma^{\mathcal{R}_i}\middle| \begin{matrix}(1,1)\\ (\mathcal{S}_i,1),(0,1)\end{matrix}\right] d\gamma = Z_2^{-(\breve{a}Z_1+1)} \\ &\quad \times H_{1,0:1,1:1,1}^{1,0:1,1:1,1}\left[\begin{matrix}J_8\\ J_2\end{matrix}\middle| \begin{matrix}(0,1)\\ (0,1)\end{matrix}\middle| \begin{matrix}(1,1)\\ (\mathcal{S}_i,1),(0,1)\end{matrix}\middle| J_9, J_{10}\right], \end{aligned} \tag{21}$$

where $Z_1 = q_1 + e_1$, $Z_2 = K_3 + M_3$, $J_8 = (-\breve{a}Z_1; 1, \mathcal{R}_i)$, $J_9 = \frac{1}{Z_2}$, and $J_{10} = \frac{\mathcal{Q}_i}{Z_2^{\mathcal{R}_i}}$.

B. EXACT SECRECY OUTAGE PROBABILITY ANALYSIS

The SOP is defined as the probability at which the instantaneous secrecy capacity (C_o) [33] drops below a target secrecy rate (τ_o). Hence, the SOP of mixed RF-UOWC network under the malicious attack of an eavesdropper is expressed as [54, Eq. (14)]

$$\begin{aligned} SOP_E &= Pr\{C_o \le \tau_o\} \\ &= Pr\{\gamma_{eq} \le \varphi\,\gamma_E + \varphi - 1\} \\ &= \int_0^\infty F_{\gamma_{eq}}(\varphi\,\gamma + \varphi - 1) f_{\gamma_E}(\gamma)\, d\gamma. \end{aligned} \tag{22}$$

Substituting (10) and (13) into (22), exact SOP is derived as

$$SOP_E = 1 - \sum_{q_1=0}^{C_R-1} M_1\, p_4 \left(\sum_{n_1=0}^{q_1} \mathcal{X}_1 - \sum_{i=1}^{q} \mathcal{P}_i\, \mathcal{X}_2\right). \tag{23}$$

Now, the derivations of the two integral terms $\mathcal{X}_1$ and $\mathcal{X}_2$ are described as follows.

1) DERIVATION OF $\mathcal{X}_1$

$\mathcal{X}_1$ is written as

$$\mathcal{X}_1 = \int_0^\infty (\varphi - 1 + \varphi\,\gamma)^{\breve{a}\,q_1}\, \gamma^{M_2}\, e^{-M_3\,\gamma^{\breve{b}}} e^{-K_3(\varphi-1+\varphi\,\gamma)^{\breve{a}}}\, d\gamma. \tag{24}$$

As (24) is mathematically intractable to solve, we assume $a_R = 2$ in (24). Now utilizing the following identity of [41, Eq. (1.111)] to evaluate $(s+k)^w = \sum_{t=0}^{w} \binom{w}{t} s^{w-t} k^{\,t}$ and performing integration with some mathematical manipulations followed by [48, Eqs. (8.4.3.1) and (2.24.1.1)], $\mathcal{X}_1$ is rewritten as

$$\begin{aligned} \mathcal{X}_1 &= \int_0^\infty \gamma^{n_1+M_2}\, e^{-p_3\,\gamma}\, e^{-M_3\,\gamma^{\breve{b}}}\, d\gamma \\ &= \int_0^\infty \gamma^{n_1+M_2}\, G_{0,1}^{1,0}\left[p_3\,\gamma\middle| \begin{matrix}-\\ 0\end{matrix}\right] G_{0,1}^{1,0}\left[M_3\,\gamma^{\breve{b}}\middle| \begin{matrix}-\\ 0\end{matrix}\right] d\gamma \\ &= \frac{\breve{b}^{\frac{1}{2}+n_1+M_2}}{p_3^{n_1+M_2+1}(2\pi)^{\frac{1}{2}(\breve{b}-1)}} G_{\breve{b},1}^{1,\breve{b}}\left[\frac{M_3}{p_3^{\breve{b}}\,\breve{b}^{-\breve{b}}}\middle| \begin{matrix}\vartheta_2\\ 0\end{matrix}\right], \end{aligned} \tag{25}$$

where $p_1 = \binom{a_1}{n_1}(\theta-1)^{q_1-n_1}\,\theta^{n_1}$, $p_2 = e^{-K_3(\theta-1)}$, $p_3 = K_3\,\varphi$, $p_4 = \frac{K_3^{q_1}}{q_1!}\,p_1\,p_2$, and $\vartheta_2 = \Delta(\breve{b}, -n_1 - M_2)$.

2) DERIVATION OF $\mathcal{X}_2$

Now $\mathcal{X}_2$ can be illustrated as

$$\begin{aligned} \mathcal{X}_2 = \int_0^\infty &(\varphi - 1 + \varphi\,\gamma)^{\breve{a}q_1}\, e^{-K_3(\varphi-1+\varphi\,\gamma)^{\breve{a}}}\, \gamma^{M_2} \\ &\times e^{-M_3\,\gamma^{\breve{b}}}\, G_{1,2}^{1,1}\left[\mathcal{Q}_i\,\gamma^{\mathcal{R}_i}\middle| \begin{matrix}1\\ \mathcal{S}_i, 0\end{matrix}\right] d\gamma. \end{aligned} \tag{26}$$

Utilizing the similar identities from $\mathcal{X}_1$ and $\Im_2$, $\mathcal{X}_2$ is expressed in an alternative form as

$$\begin{aligned} \mathcal{X}_2 &= \int_0^\infty \gamma^{n_1+M_2}\, e^{-p_3\gamma}\, e^{-M_3\,\gamma^{\breve{b}}}\, G_{1,2}^{1,1}\left[p_5\gamma^{n_2}\middle| \begin{matrix}1\\ \mathcal{S}_i, 0\end{matrix}\right] d\gamma \\ &= \int_0^\infty \gamma^{n_1+M_2}\, H_{0,1}^{1,0}\left[p_3\,\gamma\middle| \begin{matrix}-\\ (0,1)\end{matrix}\right] H_{0,1}^{1,0}\left[M_3\,\gamma^{\breve{b}}\middle| \begin{matrix}-\\ (0,1)\end{matrix}\right] \\ &\quad \times H_{1,2}^{1,1}\left[p_5\,\gamma^{n_2}\middle| \begin{matrix}(1,1)\\ (\mathcal{S}_i,1),(0,1)\end{matrix}\right] d\gamma = p_3^{-(n_1+M_2+1)} \\ &\quad \times H_{1,0:0,1:1,2}^{1,0:1,0:1,1}\left[\begin{matrix}J_{11}\\ J_2\end{matrix}\middle| \begin{matrix}-\\ (0,1)\end{matrix}\middle| \begin{matrix}(1,1)\\ (\mathcal{S}_i,1),(0,1)\end{matrix}\middle| J_{12}, J_{13}\right], \end{aligned} \tag{27}$$

where $p_5 = \mathcal{Q}_i \sum_{n_2=0}^{\mathcal{R}_i} \binom{\mathcal{R}_i}{n_2} (\theta-1)^{\mathcal{R}_i-n_2}\,\theta^{n_2}$, $J_{11} = (-n_1 - M_2; \breve{b}, n_2)$, $J_{12} = \frac{M_3}{p_3^{\breve{b}}}$, and $J_{13} = \frac{p_5}{p_3^{n_2}}$.

C. LOWER BOUND OF SECRECY OUTAGE PROBABILITY ANALYSIS

The lower bound of SOP can be obtained as

$$\begin{aligned} SOP_E \ge SOP_L &= Pr\{\gamma_{eq} \le \varphi\,\gamma_E\} \\ &= \int_0^\infty F_{\gamma_{eq}}(\varphi\,\gamma) f_{\gamma_E}(\gamma)\, d\gamma. \end{aligned} \tag{28}$$

By replacing (10) and (13) into (28), SOP is derived as

$$SOP_L = 1 - \frac{C_E^{C_E}}{\phi_R^{C_E}\,\Gamma(C_E)} \sum_{q_1=0}^{C_R-1} \frac{K_3^{q_1}}{q_1!} \varphi^{\breve{a}\,q_1} \left(\Re_1 - \sum_{i=1}^{2} \mathcal{P}_i\,\Re_2\right), \tag{29}$$

where derivations of the two integral terms $\Re_1$ and $\Re_2$ are shown as follows.

1) DERIVATION OF $\Re_1$

$\Re_1$ can be written as

$$\Re_1 = \int_0^\infty \gamma^{\breve{a}q_1+M_2}\, e^{-M_3\gamma^{\breve{b}}}\, e^{-K_3\varphi^{\breve{a}}\gamma^{\breve{a}}}\, d\gamma. \tag{30}$$

Following some mathematical manipulations defined in [55] and using identities [48, Eqs. (8.4.3.1) and (2.24.1.1)], $\Re_1$ is finally derived as

$$\begin{aligned}
\Re_1 &= \int_0^\infty \gamma^{\frac{\breve{a}q_1+M_2}{\breve{a}}} e^{-M_3\gamma^{\frac{\breve{b}}{\breve{a}}}} e^{-K_3\varphi^{\breve{a}}\gamma} d(\gamma^{\frac{1}{\breve{a}}}) \\
&= \frac{1}{\breve{a}}\int_0^\infty \gamma^{\vartheta_3-1} e^{-K_3\varphi^{\breve{a}}\gamma} e^{-M_3\gamma^{\frac{\breve{b}}{\breve{a}}}} d\gamma \\
&= \frac{1}{\breve{a}}\int_0^\infty \gamma^{\vartheta_3-1} G_{0,1}^{1,0}\left[K_3\varphi^{\breve{a}}\gamma \middle| \begin{matrix} - \\ 0 \end{matrix}\right] G_{0,1}^{1,0}\left[M_3\gamma^{\frac{\breve{b}}{\breve{a}}} \middle| \begin{matrix} - \\ 0 \end{matrix}\right] d\gamma \\
&= \frac{\breve{b}^{\vartheta_3-\frac{1}{2}}(K_3\varphi^{\breve{a}})^{-\vartheta_3}}{\breve{a}^{\frac{1}{2}}(2\pi)^{\frac{1}{2}(\breve{a}+\breve{b}-2)}} G_{\breve{b},\breve{a}}^{\breve{a},\breve{b}}\left[\frac{M_3^{\breve{a}}\breve{a}^{-\breve{a}}}{(K_3\varphi^{\breve{a}})^{\breve{b}}\breve{b}^{-\breve{b}}} \middle| \begin{matrix} \vartheta_4 \\ 0 \end{matrix}\right],
\end{aligned} \tag{31}$$

where $\vartheta_3 = \frac{\breve{a}q_1+M_2+1}{\breve{a}}$ and $\vartheta_4 = \Delta(\breve{b}, 1-\vartheta_3)$.

2) DERIVATION OF $\Re_2$

$\Re_2$ can be derived as

$$\begin{aligned}
\Re_2 = &\int_0^\infty \gamma^{M_2+\breve{a}q_1} e^{-M_3\gamma^{\breve{b}}} e^{-K_3(\gamma\varphi)^{\breve{a}}} \\
&\times G_{1,2}^{1,1}\left[\mathcal{Q}_i(\varphi\gamma)^{\mathcal{R}_i} \middle| \begin{matrix} 1 \\ \mathcal{S}_i, 0 \end{matrix}\right] d\gamma.
\end{aligned} \tag{32}$$

As the solution of (32) is mathematically intractable, we assume $b_E = 2$ for deriving $\Re_2$ with the help of [50, Eq. (6.2.8)], [51, Eq. (2.3)], and [52, Eq. (3)] as follows

$$\begin{aligned}
\Re_2 = &\int_0^\infty \gamma^{M_2+\breve{a}q_1} e^{-M_3\gamma} e^{-K_3(\gamma\varphi)^{\breve{a}}} \\
&\times G_{1,2}^{1,1}\left[\mathcal{Q}_i(\varphi\gamma)^{\mathcal{R}_i} \middle| \begin{matrix} 1 \\ \mathcal{S}_i, 0 \end{matrix}\right] d\gamma \\
= &\int_0^\infty \gamma^{\breve{a}q_1+C_E-1} H_{0,1}^{1,0}\left[M_3\gamma \middle| \begin{matrix} - \\ (0,1) \end{matrix}\right] \\
&\times H_{0,1}^{1,0}\left[K_3(\varphi\gamma)^{\breve{a}} \middle| \begin{matrix} - \\ (0,1) \end{matrix}\right] \\
&\times H_{1,2}^{1,1}\left[\mathcal{Q}_i(\varphi\gamma)^{\mathcal{R}_i} \middle| \begin{matrix} (1,1) \\ (\mathcal{S}_i,1),(0,1) \end{matrix}\right] d\gamma = M_3^{-(\breve{a}q_1+C_E)} \\
&\times H_{1,0:0,1:1,2}^{1,0:1,0:1,1}\left[\begin{matrix} J_{14} \\ J_2 \end{matrix} \middle| \begin{matrix} - \\ (0,1) \end{matrix} \middle| \begin{matrix} (1,1) \\ (\mathcal{S}_i,1),(0,1) \end{matrix} \middle| J_{15}, J_{16}\right],
\end{aligned} \tag{33}$$

where $J_{14} = (1-\breve{a}q_1-C_E; \breve{a}, \mathcal{R}_i)$, $J_{15} = \frac{K_3\varphi^{\breve{a}}}{M_3^{\breve{a}}}$, and $J_{16} = \frac{\mathcal{Q}_i\varphi^{\mathcal{R}_i}}{M_3^{\mathcal{R}_i}}$.

D. STRICTLY POSITIVE SECRECY CAPACITY ANALYSIS

The SPSC is a significant parameter in wiretapped model that assures an uninterrupted communication which is feasible only if the secrecy capacity remains as a positive quantity. Mathematically, it is given as [56, Eq. (25)]

$$\begin{aligned}
SPSC &= Pr\{C_o > 0\} \\
&= 1 - Pr\{C_o \le 0\} \\
&= 1 - SOP_L(\tau_o = 0).
\end{aligned} \tag{34}$$

With the help of (34), the probability of SPSC can be obtained. Therefore, substituting $\tau_o = 0$ in (29), the analytical expression of SPSC is finally determined as expressed in (35), as shown at the bottom of the next page.

IV. NUMERICAL RESULTS

This section illustrates the impact of various system parameters on the secrecy performance of the proposed mixed RF-UOWC system via different numerical examples utilizing the expressions in (15), (23), (29), and (35). MC simulation is carried out to confirm the accuracy of the novel expressions by generating 10^6 random samples in MATLAB. The simulation results are labelled as 'Sim' in all the figures. GG is randomly generated using the MATLAB gamrnd(.) function while bivariate Fox's H function is computed and implemented following the approach outlined in [52, Table I]. Although we consider $a_R = b_E$ in (20), $a_R = 2$ in (24), (26), and $b_E = 2$ in (32) to satisfy some mathematical identities, the effects of a_R and b_E in some of the numerical examples are observed via numerical approach with no loss of generality. We utilize various UWTs from Tables 2 and 3 to assess the degree of impact of UWT via temperature gradient and thermally uniform UOWC channels.

The effect of fading severity parameters (i.e. a_R, b_E, C_R, and C_E) on the system's ASC and lower bound of SOP performance as a function of ϕ_R is presented in Figs. 2, 3, and 4. In each of these examinations, we assume two different cases of ϕ_E (i.e. ϕ_E= 0 dB and 3 dB). The results indicate that ASC improves with an increase in a_R and C_R. This happens because the fading of $S-R$ becomes less severe with the increase of a_R and C_R that leads to an enhanced system performance as verified in [56]. In contrast, the increase in ϕ_E depreciates the secrecy capacity. Similarly, an increase in b_E and C_E improves the $S-E$ link quality that in turn increases the lower bound of SOP. In each figure, we also show some simulated results along with the respective analytical results. It is clearly observed that the two results match completely with one another. The observation therefore implies the exactitude of our developed expressions in (15) and (29). Note that whereas we notice an ASC ceiling in Figs. 2 and 3, a SOP floor is visible in Fig. 4. This is due to the bottleneck that occurs mostly because of the limitations at the RF hop.

The SPSC versus μ_r performance is summarized in Fig. 5 for different values of ϕ_E. Clearly, we can remark that the SPSC gradually declines when ϕ_E changes from a weak (−6dB) to a stronger (2dB) conditions. As an increased ϕ_E represents a stronger wiretap channel, the SPSC degrades with an increase in ϕ_E. A close agreement between MC simulations and analytical results reveal that the SPSC expression in (35) is accurate.

Figure 6 portrays the influence of μ_r on SPSC performance with HD detection (i.e. $r = 1$). It can be summarized that

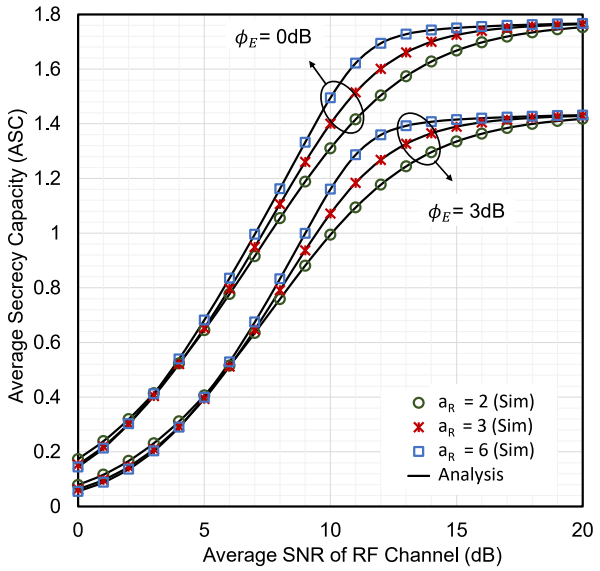

FIGURE 2. The ASC versus ϕ_R for selected values of a_R and ϕ_E with $b_E = C_R = C_E = 2$, $h = 2.4$, $l = 0.05$, $r = 1$, and $\phi_U = 10$ dB.

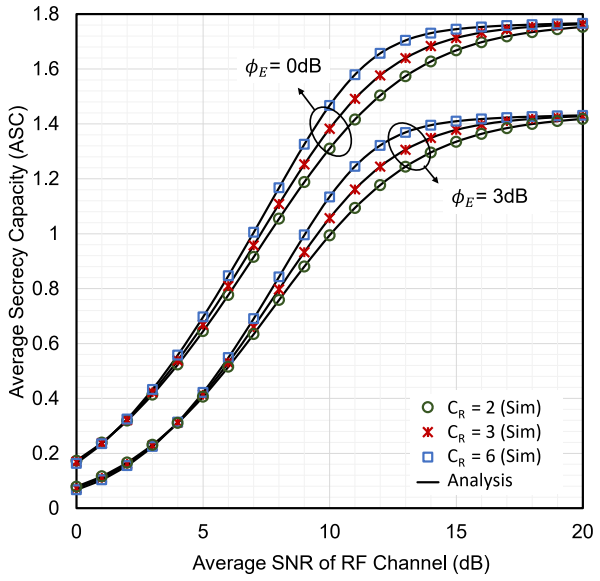

FIGURE 3. The ASC versus ϕ_R for selected values of C_R and ϕ_E with $a_R = b_E = C_E = 2$, $h = 2.4$, $l = 0.05$, $r = 1$, and $\phi_U = 10$ dB.

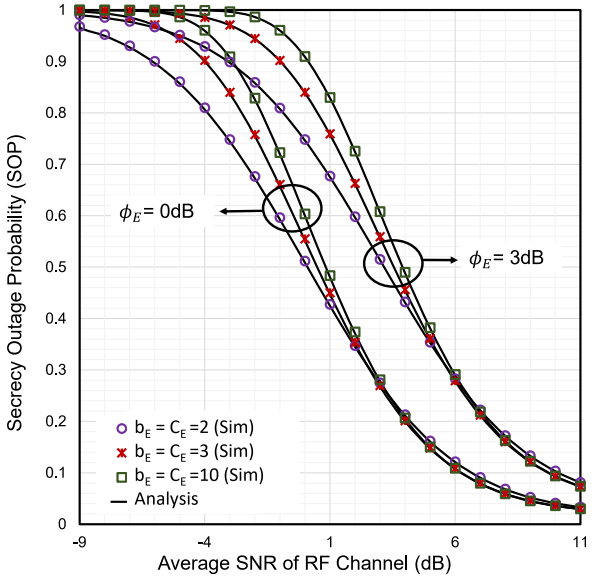

FIGURE 4. The lower bound of SOP versus ϕ_R for selected values of b_E, C_E, and ϕ_E with $a_R = C_R = 2$, $h = 2.4$, $l = 0.05$, $r = 1$, $\phi_U = 15$ dB, and $\tau_o = 0.01$ bits/s/Hz.

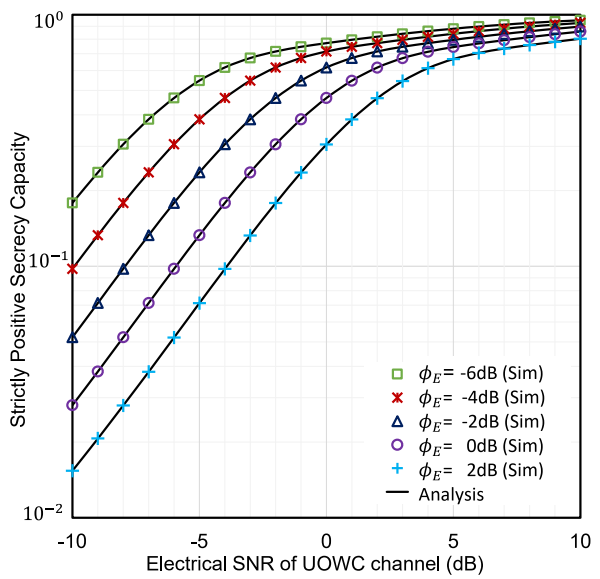

FIGURE 5. The SPSC versus μ_r for selected values of ϕ_E with $a_R = C_R = 3$, $b_E = C_E = 2$, $h = 4.7$, $l = 0.1$, $r = 1$, and $\phi_R = 10$ dB.

the higher the value of μ_r becomes, the higher the SPSC is. The results is desirable as a larger value of μ_r strengthens the $R - U$ link quality, verified in [37]. In addition, this figure reveals that system behavior alters rapidly at lower ϕ_R relative to higher ϕ_R resulting in a SPSC ceiling at each curve.

Figures 7, 8, and 9 present the SOP versus ϕ_R to explain various UWT situations. Fig. 7 demonstrates a salty

$$SPSC = \frac{C_E^{C_E}}{\phi_R^{C_E}\,\Gamma(C_E)} \sum_{q_1=0}^{C_R-1} \frac{K_3^{q_1}}{q_1!} \left(\frac{\breve{b}^{\vartheta_2-\frac{1}{2}}(K_3)^{-\vartheta_2}}{\breve{a}^{\frac{1}{2}}(2\pi)^{\frac{1}{2}(\breve{a}+\breve{b}-2)}} G_{\breve{b},\breve{a}}^{\breve{a},\breve{b}} \left[\frac{M_3^{\breve{a}}\breve{a}^{-\breve{a}}}{(K_3)^{\breve{b}}\breve{b}^{-\breve{b}}} \middle| \begin{matrix} \vartheta_4 \\ 0 \end{matrix} \right] - \sum_{i=1}^{2} \mathcal{P}_i M_3^{-(\breve{a}q_1+C_E)} \right.$$
$$\left. \times H_{1,0:0,1:1,2}^{1,0:1,0:1,1} \left[\begin{matrix} J_{11} \\ J_2 \end{matrix} \middle| \begin{matrix} - \\ (0,1) \end{matrix} \middle| \begin{matrix} (1,1) \\ (\mathcal{S}_i,1),(0,1) \end{matrix} \middle| \begin{matrix} K_3 \\ M_3^{\breve{a}} \end{matrix}, \frac{\mathcal{Q}_i}{M_3^{\mathcal{R}_i}} \right] \right). \tag{35}$$

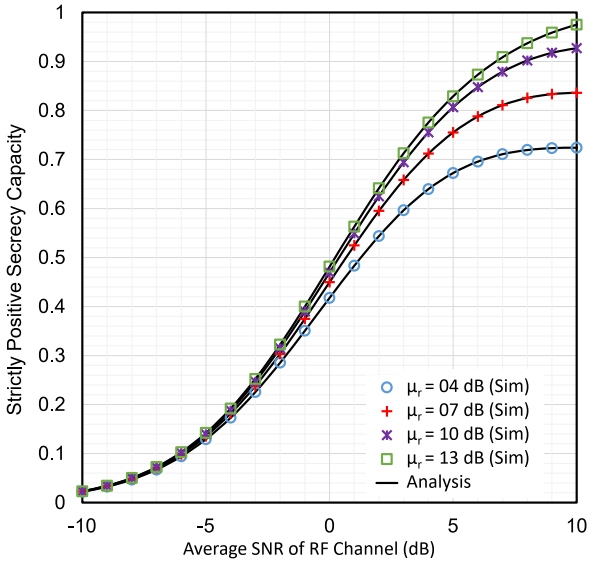

FIGURE 6. The SPSC versus ϕ_R for selected values of μ_r with $a_R = b_E = C_R = C_E = 2$, $h = 4.7$, $l = 0.1$, $r = 1$, and $\phi_E = 0$ dB.

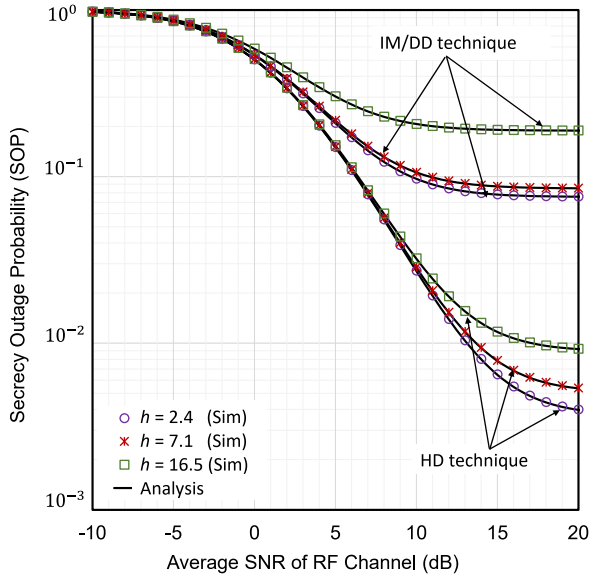

FIGURE 7. The lower bound of SOP versus ϕ_R for selected values of h and r with $a_R = b_E = C_R = C_E = 2$, $\phi_U = 20$ dB, $\phi_E = 0$ dB, and $\tau_o = 0.01$ bits/s/Hz.

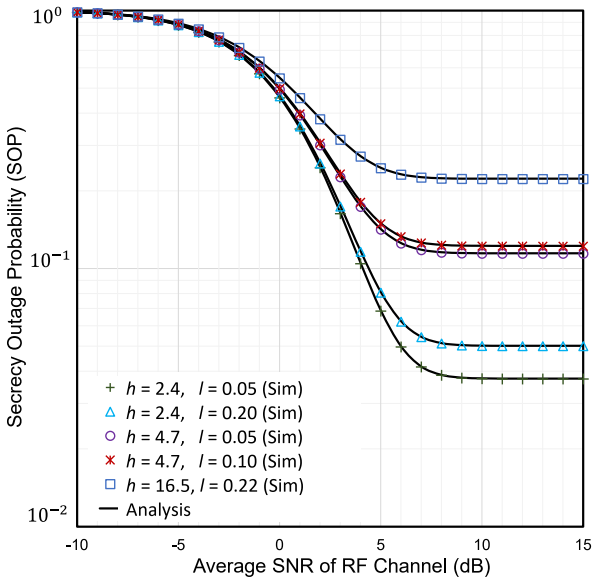

FIGURE 8. The lower bound of SOP versus ϕ_R for selected values of h and l with $a_R = C_R = 4$, $b_E = C_E = 2$, $r = 2$, $\phi_U = 30$ dB, $\phi_E = 0$ dB, and $\tau_o = 0.01$ bits/s/Hz.

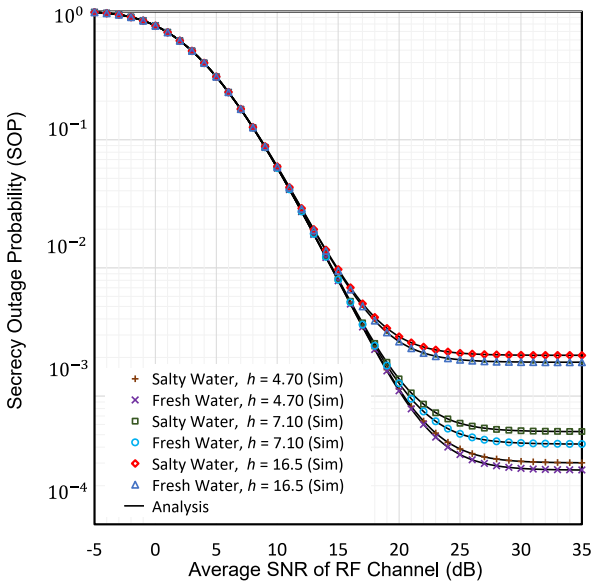

FIGURE 9. The exact SOP versus ϕ_R for selected values of h with $a_R = b_E = C_R = C_E = 2$, $r = 1$, $\phi_U = 30$ dB, $\phi_E = 0$ dB, and $\tau_o = 0.5$ bits/s/Hz.

thermally uniform UOWC channel wherein the HD technique overcomes UWT more efficiently compared to the IM/DD technique since the received SNR at U is higher for the former. The UWT increases with both h and l in a temperature gradient UOWC channel as demonstrated in Fig. 8 for which the SOP degrades with increasing h and l. This clearly indicates that an increase in temperature gradient introduces acute irradiance fluctuations which in turn increases the scintillation index as well as UWT. In Fig. 9, a thermally uniform condition with various levels of air bubbles for both types of water (i.e. fresh and salty) is considered and it is seen that with the increase in UWT (i.e. increased h in salty and fresh water), the exact SOP also increases. Similar conclusions were established in [26] that confirms the tightness of our analysis.

In Fig. 10, the exact SOP is depicted against ϕ_U to quantify the effect of τ_o. It is noted that the SOP deteriorates consistently with the increase of τ_o. To establish a reliable communication over the RF-UOWC link, C_0 must be greater than τ_o. But if τ_o is set to a higher value, the probability that C_0 will drop below τ_o will increase and hence the SOP will degrade.

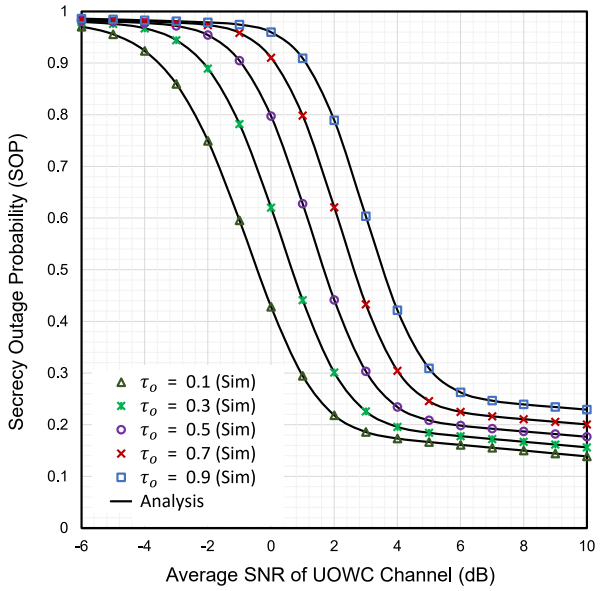

FIGURE 10. The exact SOP versus ϕ_U for selected values of τ_o with $a_R = C_R = 2$, $b_E = C_E = 3$, $h = 2.4$, $l = 0.1$, $r = 2$, $\phi_R = 10$ dB, and $\phi_E = 0$ dB.

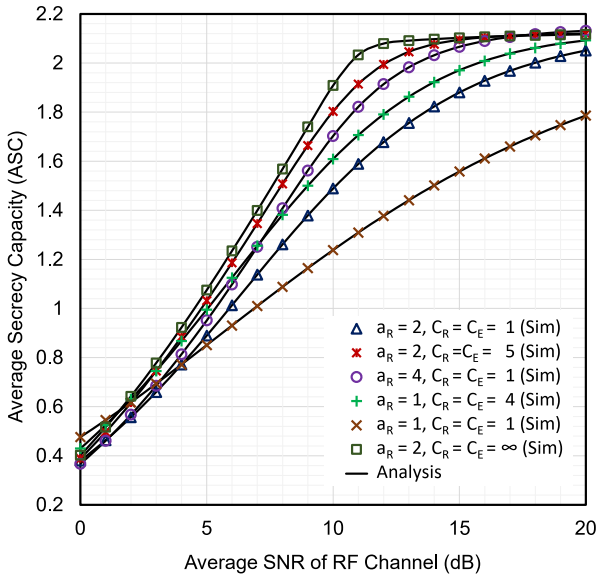

FIGURE 11. The ASC versus ϕ_R for selected values of a_R, C_R, and C_E with $b_E = 2$, $h = 2.4$, $l = 0.05$, $r = 1$, $\phi_U = 10$ dB, and $\phi_E = -5$ dB.

Generalization offered by the proposed model:

As the considered distributions of the RF and UOWC links are generalized, numerous classical RF and UOWC models can be demonstrated as special scenarios of the proposed work. For instance, performance unification of all the RF channels as illustrated in Table 1 can be easily performed utilizing GG fading channel. This generic characteristics are exhibited in Fig. 11 for better realization of all the channel parameters corresponding to each individual special case models. In addition, for $c = 1$, the mEGG is transformed into well-known EG distribution.

Additionally, this work consolidates the evaluation of secrecy performances over a wide range of existing classical RF and UOWC mixed models considering both thermally uniform and temperature gradient UOWC channels subjected to different forms of UWT in fresh and salty water environment. As such, we arguably conclude that the proposed model exhibits significant novelty in secrecy analysis over all the existing RF-UOWC mixed networks.

V. CONCLUDING REMARKS

In this research, we examined the secrecy performance of a dual-hop RF-UOWC system exploiting the physical properties of the RF and UOWC channels. The implementation of generalized distributions in both the links exhibits enormous versatility over existing works because the derived generalized expressions of the secrecy metrics (i.e. SPSC, ASC, and SOP) can reliably explain the secrecy behaviour of existing classical models. An exact match of numerical results with the MC simulations validates the accuracy of the derivations. Our results demonstrate that the HD technique is a more convenient approach for secure communication compared to the IM/DD technique. Moreover, the impact of RF channel fading parameters, air bubble level with temperature gradient, and thermally uniform conditions in both the salty and fresh water environments is also investigated. Besides air bubbles, increasing temperature gradient imposes significant detrimental impact on the secrecy performance, concluded on the basis of numerical results. In future, this work can be extended considering simultaneous eavesdropping via both RF and UOWC links.

REFERENCES

[1] M. Stojanovic and J. Preisig, "Underwater acoustic communication channels: Propagation models and statistical characterization," *IEEE Commun. Mag.*, vol. 47, no. 1, pp. 84–89, Jan. 2009.

[2] I. F. Akyildiz, P. Wang, and Z. Sun, "Realizing underwater communication through magnetic induction," *IEEE Commun. Mag.*, vol. 53, no. 11, pp. 42–48, Nov. 2015.

[3] H. Kaushal and G. Kaddoum, "Underwater optical wireless communication," *IEEE Access*, vol. 4, pp. 1518–1547, 2016.

[4] B. Cochenour, A. Laux, and L. Mullen, "Temporal dispersion in underwater laser communication links: Closing the loop between model and experiment," in *Proc. IEEE 3rd Underwater Commun. Netw. Conf. (UComms)*, Aug. 2016, pp. 1–5.

[5] I. S. Ansari, M. M. Abdallah, M.-S. Alouini, and K. A. Qaraqe, "A performance study of two hop transmission in mixed underlay RF and FSO fading channels," in *Proc. IEEE Wireless Commun. Netw. Conf. (WCNC)*, Apr. 2014, pp. 388–393.

[6] E. Illi, F. El Bouanani, and F. Ayoub, "A high accuracy solver for RTE in underwater optical communication path loss prediction," in *Proc. Int. Conf. Adv. Commun. Technol. Netw. (CommNet)*, Apr. 2018, pp. 1–8.

[7] Z. Zeng, "A survey of underwater wireless optical communication," Ph.D. dissertation, Dept. Elect. Eng., Univ. British Columbia, Vancouver, BC, Canada 2015.

[8] M. V. Jamali, J. A. Salehi, and F. Akhoundi, "Performance studies of underwater wireless optical communication systems with spatial diversity: MIMO scheme," *IEEE Trans. Commun.*, vol. 65, no. 3, pp. 1176–1192, Dec. 2016.

[9] C. Gabriel, M.-A. Khalighi, S. Bourennane, P. Leon, and V. Rigaud, "Monte-Carlo-based channel characterization for underwater optical communication systems," *J. Opt. Commun. Netw.*, vol. 5, no. 1, pp. 1–12, 2013.

[10] F. Akhoundi, M. V. Jamali, N. B. Hassan, H. Beyranvand, A. Minoofar, and J. A. Salehi, "Cellular underwater wireless optical CDMA network: Potentials and challenges," *IEEE Access*, vol. 4, pp. 4254–4268, 2016.
[11] H. M. Oubei, R. T. ElAfandy, K.-H. Park, T. K. Ng, M.-S. Alouini, and B. S. Ooi, "Performance evaluation of underwater wireless optical communications links in the presence of different air bubble populations," *IEEE Photon. J.*, vol. 9, no. 2, Apr. 2017, Art. no. 7903009.
[12] M.-A. Khalighi, T. Hamza, S. Bourennane, P. Leon, and J. Opderbecke, "Underwater wireless optical communications using silicon photomultipliers," *IEEE Photon. J.*, vol. 9, no. 4, Aug. 2017, Art. no. 7905310.
[13] W. Wang, P. Wang, T. Cao, H. Tian, Y. Zhang, and L. Guo, "Performance investigation of underwater wireless optical communication system using M-ary OAMSK modulation over oceanic turbulence," *IEEE Photon. J.*, vol. 9, no. 5, Oct. 2017, Art. no. 7905315.
[14] E. Zedini, H. M. Oubei, A. Kammoun, M. Hamdi, B. S. Ooi, and M.-S. Alouini, "A new simple model for underwater wireless optical channels in the presence of air bubbles," in *Proc. IEEE Global Commun. Conf.*, Dec. 2017, pp. 1–6.
[15] F. Hanson and S. Radic, "High bandwidth underwater optical communication," *Appl. Opt*, vol. 47, no. 2, pp. 277–283, 2008.
[16] J. Xu, M. Kong, A. Lin, Y. Song, X. Yu, F. Qu, J. Han, and N. Deng, "OFDM-based broadband underwater wireless optical communication system using a compact blue LED," *Opt. Commun.*, vol. 369, pp. 100–105, Jun. 2016.
[17] S. Arnon and D. Kedar, "Non-line-of-sight underwater optical wireless communication network," *J. Opt. Soc. Amer. A, Opt. Image Sci.*, vol. 26, no. 3, pp. 530–539, 2009.
[18] M. V. Jamali, A. Chizari, and J. A. Salehi, "Performance analysis of multihop underwater wireless optical communication systems," *IEEE Photon. Technol. Lett.*, vol. 29, no. 5, pp. 462–465, Mar. 1, 2017.
[19] S. Jaruwatanadilok, "Underwater wireless optical communication channel modeling and performance evaluation using vector radiative transfer theory," *IEEE J. Sel. Areas Commun.*, vol. 26, no. 9, pp. 1620–1627, Dec. 2008.
[20] O. Korotkova, N. Farwell, and E. Shchepakina, "Light scintillation in oceanic turbulence," *Waves Random Complex Media*, vol. 22, no. 2, pp. 260–266, May 2012.
[21] H. M. Oubei, E. Zedini, R. T. ElAfandy, A. Kammoun, T. K. Ng, M.-S. Alouini, and B. S. Ooi, "Efficient weibull channel model for salinity induced turbulent underwater wireless optical communications," in *Proc. Opto-Electron. Commun. Conf. (OECC) Photon. Global Conf. (PGC)*, Jul. 2017, pp. 1–2.
[22] H. Oubei, E. Zedini, R. ElAfandy, and A. Kammoun, "Simple statistical channel model for weak temperature-induced turbulence in underwater wireless optical communication systems," *Opt. Lett.*, vol. 42, no. 13, pp. 2455–2458, 2017.
[23] K. P. Peppas, A. C. Boucouvalas, and Z. Ghassemloy, "Performance of underwater optical wireless communication with multi-pulse pulse-position modulation receivers and spatial diversity," *IET Optoelectron.*, vol. 11, no. 5, pp. 180–185, Oct. 2017.
[24] N. Farr, A. Bowen, J. Ware, C. Pontbriand, and M. Tivey, "An integrated, underwater optical/acoustic communications system," in *Proc. OCEANS*, May 2010, pp. 1–6.
[25] W. Liu, Z. Xu, and L. Yang, "SIMO detection schemes for underwater optical wireless communication under turbulence," *Photon. Res.*, vol. 3, no. 3, pp. 48–53, Oct. 2015.
[26] E. Zedini, H. M. Oubei, A. Kammoun, M. Hamdi, B. S. Ooi, and M.-S. Alouini, "Unified statistical channel model for turbulence-induced fading in underwater wireless optical communication systems," *IEEE Trans. Commun.*, vol. 67, no. 4, pp. 2893–2907, Apr. 2019.
[27] Z. Zeng, S. Fu, H. Zhang, Y. Dong, and J. Cheng, "A survey of underwater optical wireless communications," *IEEE Commun. Surveys Tuts.*, vol. 19, no. 1, pp. 204–238, 1st Quart., 2017.
[28] E. Illi, F. El Bouanani, D. B. Da Costa, F. Ayoub, and U. S. Dias, "Dual-hop mixed RF-UOW communication system: A PHY security analysis," *IEEE Access*, vol. 6, pp. 55345–55360, 2018.
[29] S. Anees and R. Deka, "On the performance of DF based dual-hop mixed RF/UWOC system," in *Proc. IEEE 89th Veh. Technol. Conf. (VTC-Spring)*, Apr. 2019, pp. 1–5.
[30] M. Amer and Y. Al-Eryani, "Underwater optical communication system relayed by α-μ fading channel: Outage, capacity and asymptotic analysis," 2019, *arXiv:1911.04243*. [Online]. Available: http://arxiv.org/abs/1911.04243
[31] H. Lei, Y. Zhang, K.-H. Park, I. S. Ansari, G. Pan, and M.-S. Alouini, "Performance analysis of dual-hop RF-UWOC systems," *IEEE Photon. J.*, vol. 12, no. 2, pp. 1–15, Apr. 2020.
[32] H. Lei, Y. Zhang, K.-H. Park, I. S. Ansari, G. Pan, and M.-S. Alouini, "Performance analysis of dual-hop RF-UWOC systems," *IEEE Photon. J.*, vol. 12, no. 2, Apr. 2020, Art. no. 7901915.
[33] A. D. Wyner, "The wire-tap channel," *Bell Syst. Tech. J.*, vol. 54, no. 8, pp. 1355–1387, Oct. 1975.
[34] H. Yu, T. Kim, and H. Jafarkhani, "Wireless secure communication with beamforming and jamming in time-varying wiretap channels," *IEEE Trans. Inf. Forensics Security*, vol. 13, no. 8, pp. 2087–2100, Aug. 2018.
[35] H. Yu and I.-G. Lee, "Physical layer security based on NOMA and AJ for MISOSE channels with an untrusted relay," *Future Gener. Comput. Syst.*, vol. 102, pp. 611–618, Jan. 2020.
[36] E. Illi, F. E. Bouanani, D. B. da Costa, F. Ayoub, and U. S. Dias, "On the secrecy performance of mixed RF/UOW communication system," in *Proc. IEEE Globecom Workshops (GC Wkshps)*, Dec. 2018, pp. 1–6.
[37] E. Illi, F. El Bouanani, D. Benevides da Costa, P. C. Sofotasios, F. Ayoub, K. Mezher, and S. Muhaidat, "Physical layer security of a dual-hop regenerative mixed RF/UOW system," *IEEE Trans. Sustain. Comput.*, early access, Mar. 26, 2020, doi: 10.1109/TSUSC.2019.2906545.
[38] P. S. Bithas, N. C. Sagias, and P. T. Mathiopoulos, "Gsc diversity receivers over generalized-Gamma fading channels," *IEEE Commun. Lett.*, vol. 11, no. 12, pp. 964–966, 2007.
[39] M. O. Hasna and M.-S. Alouini, "A performance study of dual-hop transmissions with fixed gain relays," in *Proc. IEEE Int. Conf. Acoust., Speech, Signal Process. (ICASSP)*, Apr. 2003, pp. 189–192.
[40] H. Lei, C. Gao, Y. Guo, and G. Pan, "On physical layer security over generalized Gamma fading channels," *IEEE Commun. Lett.*, vol. 19, no. 7, pp. 1257–1260, Jul. 2015.
[41] A. Jeffrey and D. Zwillinger, *Table of Integrals, Series, and Products*. Amsterdam, The Netherlands: Elsevier, 2007.
[42] P. M. Shankar, *Fading and Shadowing in Wireless Systems*. Cham, Switzerland: Springer, 2017.
[43] M. Khodabina and A. Ahmadabadib, "Some properties of generalized Gamma distribution," *Math. Sci.*, vol. 4, no. 1, pp. 9–28, Mar. 2010.
[44] I. S. Ansari, F. Yilmaz, and M.-S. Alouini, "On the sum of squared eta-μ random variates with application to the performance of wireless communication systemss," in *Proc. IEEE 77th Veh. Technol. Conf. (VTC Spring)*, Jun. 2013, pp. 1–6.
[45] A. C. Boucouvalas, K. P. Peppas, K. Yiannopoulos, and Z. Ghassemlooy, "Underwater optical wireless communications with optical amplification and spatial diversity," *IEEE Photon. Technol. Lett.*, vol. 28, no. 22, pp. 2613–2616, Nov. 15, 2016.
[46] K. O. Odeyemi and P. A. Owolawi, "Impact of non-zero boresight pointing errors on multiuser mixed RF/FSO system under best user selection scheme," *Int. J. Microw. Opt. Technol*, vol. 14, no. 3, pp. 210–222, 2019.
[47] L. Wang, M. Elkashlan, J. Huang, R. Schober, and R. K. Mallik, "Secure transmission with antenna selection in MIMO Nakagami-*m* fading channels," *IEEE Trans. Wireless Commun.*, vol. 13, no. 11, pp. 6054–6067, Nov. 2014.
[48] A. Prudnikov, Y. Brychkov, and O. Marichev, *Integrals Series: More Special Functions*, vol. 3. London, U.K.: Gordon And Breach Science, 1992.
[49] V. S. Adamchik and O. I. Marichev, "The algorithm for calculating integrals of hypergeometric type functions and its realization in REDUCE system," in *Proc. Int. Symp. Symbolic Algebr. Comput.*, 1990, pp. 212–224.
[50] M. D. Springer, *The Algebra of Random Variables* (Wiley Series in Probability and Mathematical Statistics). New York, NY, USA: Wiley, 1979, p. 470.
[51] P. K. Mittal and K. C. Gupta, "An integral involving generalized function of two variables," *Proc. Indian Acad. Sci.*, vol. 75, no. 3, pp. 117–123, 1972.
[52] H. Lei, I. S. Ansari, G. Pan, B. Alomair, and M.-S. Alouini, "Secrecy capacity analysis over $\alpha - \mu$ fading channels," *IEEE Commun. Lett.*, vol. 21, no. 6, pp. 1445–1448, Jun. 2017.
[53] A. M. Mathai, R. K. Saxena, and H. J. Haubold, *The H-Function: Theory Application*. Cham, Switzerland: Springer, 2009.

[54] H. Lei, H. Zhang, I. S. Ansari, C. Gao, Y. Guo, G. Pan, and K. A. Qaraqe, "Performance analysis of physical layer security over generalized-K fading channels using a mixture Gamma distribution," *IEEE Commun. Lett.*, vol. 20, no. 2, pp. 408–411, Feb. 2016.
[55] J. M. Moualeu, D. B. da Costa, W. Hamouda, U. S. Dias, and R. A. A. de Souza, "Physical layer security over $\alpha-\kappa-\mu$ and $\alpha-\eta-\mu$ fading channels," *IEEE Trans. Veh. Tech.*, vol. 68, no. 1, pp. 1025–1029, Jan. 2019.
[56] S. H. Islam, A. S. M. Badrudduza, S. M. Riazul Islam, F. I. Shahid, I. S. Ansari, M. K. Kundu, S. K. Ghosh, M. B. Hossain, A. S. M. S. Hosen, and G. H. Cho, "On secrecy performance of mixed generalized Gamma and Málaga RF-FSO variable gain relaying channel," *IEEE Access*, vol. 8, pp. 104127–104138, 2020.

A. S. M. BADRUDDUZA (Member, IEEE) received the B.Sc. and M.Sc. degrees in electrical & electronic engineering (EEE) from the Rajshahi University of Engineering & Technology (RUET), Rajshahi, Bangladesh, in 2016 and 2019, respectively.

From 16 September 2016 to 22 July 2017, he was a Lecturer with the Department of Electrical and Electronic Engineering (EEE), Bangladesh Army University of Engineering & Technology (BAUET), Rajshahi. From 23 July 2017 to 29 June 2020, he was a Lecturer with the Department of Electronics and Telecommunication Engineering (ETE), RUET. Since 30 June 2020, he has been an Assistant Professor with the Department of Electronics and Telecommunication Engineering (ETE), RUET. He has been affiliated with IEEE, since 2020. He is an active reviewer for several IEEE journals. He has authored/coauthored over 30 international journals/conference publications. His research interests include physical layer security in multicast, cellular and cooperative networks, free space optics (FSO), underwater optics (UWO), and NOMA systems.

Mr. Badrudduza was a recipient of two EEE Association Awards, such as the Student of the Year Award from RUET for his outstanding academic performances in the first and fourth year examinations while pursuing his B.Sc. engineering degree and two best paper awards for two different research papers from the IEEE Region 10 Symposium (TENSYMP2020), and the IEEE 3rd International Conference on Telecommunication and Photonics (ICTP2019).

MD. IBRAHIM is currently pursuing the B.Sc. degree in electrical & electronic engineering (EEE) with the Rajshahi University of Engineering & Technology (RUET), Rajshahi, Bangladesh. His research interests include RF-FSO communication, physical layer security, UWOC systems, wireless multicasting, and cognitive networks.

S. M. RIAZUL ISLAM (Member, IEEE) is currently an Assistant Professor with the Department of Computer Science and Engineering, Sejong University, South Korea. Prior to Sejong, he worked as a Postdoctoral Fellow with the Wireless Communications Research Center, Inha University, South Korea. He was also affiliated with Memorial University, Canada, as a Postdoctoral Fellow. Before that, he was with the University of Dhaka, Bangladesh, as an Assistant Professor and a Lecturer with the Department of Electrical and Electronic Engineering. He also worked with the Samsung R&D Institute Bangladesh as a Chief Engineer with the Department of Solution Laboratory for Advanced Research. His research interests include wireless communications, the Internet of Things, and applied artificial intelligence.

MD. SHAKHAWAT HOSSEN (Member, IEEE) is currently pursuing the B.Sc. degree in electronics & telecommunication engineering (ETE) with the Rajshahi University of Engineering & Technology (RUET), Rajshahi, Bangladesh. His research interests include wireless channel multicasting, physical layer security of RF-FSO, UWOC networks, and CubeSat communication sub-systems.

MILTON KUMAR KUNDU (Member, IEEE) received the B.Sc. degree in electrical & electronic engineering (EEE) from the Rajshahi University of Engineering & Technology (RUET), Rajshahi, Bangladesh, in 2016.

He has worked as a Lecturer with the Department of Electrical and Electronic Engineering (EEE), North Bengal International University, Rajshahi, from 20 May 2017 to 14 February 2019. He has been working as a Lecturer with the Department of Electrical & Computer Engineering (ECE), RUET, since 16 February 2019. He is also an Advisor of the IEEE RUET Industry Applications Society (IAS) Student Branch Chapter. His research interests include centered around the security aspects of cooperative and physical-layer networks and wireless multicasting.

Mr. Kundu has won several awards, including the Second Runner-Up Award for Regional Mathematical Olympiad, the EEE Association Award, the Student of the Year Award from RUET for his outstanding academic performances in the third year examinations while pursuing the B.Sc. engineering degree. He has also won two best paper awards for two different research papers from the IEEE Region 10 Symposium (TENSYMP 2020), and the IEEE 3rd International Conference on Telecommunication and Photonics (ICTP 2019).

IMRAN SHAFIQUE ANSARI (Member, IEEE) received the B.Sc. degree (Hons.) in computer engineering from the King Fahd University of Petroleum and Minerals (KFUPM), in 2009, and the M.Sc. and Ph.D. degrees from the King Abdullah University of Science and Technology (KAUST), in 2010 and 2015, respectively.

From May 2009 to August 2009, he was a Visiting Scholar with Michigan State University (MSU), East Lansing, MI, USA, and from June 2010 to August 2010, he was a Research Intern with Carleton University, Ottawa, ON, Canada. From April 2015 to November 2017, he was a Postdoctoral Research Associate (PRA) with Texas A&M University at Qatar (TAMUQ). From November 2017 to July 2018, he was a Lecturer (an Assistant Professor) with the Global College of Engineering and Technology (GCET) affiliated with the University of the West of England (UWE), Bristol, U.K. Since August 2018, he has been a Lecturer (an Assistant Professor) with the University of Glasgow, Glasgow, U.K. He has authored/coauthored over 100 journal and conference publications. He has co-organized the GRASNET'2016, 2017, 2018 workshops in conjunction with IEEE WCNC'2016, 2017, and IEEE Globecom 2018. His current research interests include free-space optics (FSO), channel modeling/signal propagation issues, relay/multihop communications, physical layer secrecy issues, full duplex systems, and secure D2D applications for 5G+ systems, among others.

Dr. Ansari has been affiliated with IEEE since 2007. He has served in various capacities. He has been serving for the IEEE Nominations and Appointments (N&A) Committee, from 2020 to 2021, and the IEEE Communication Society Young Professionals (ComSoc YP) Board, since April 2016. He has been a part of the IEEE 5G Tech Focus Publications Editorial Board, since February 2017. He is an active reviewer for various IEEE TRANSACTIONS and various other journals. He has served as a TPC for various IEEE conferences. He was a recipient of appreciation for an Exemplary Reviewer for IEEE TRANSACTION ON COMMUNICATIONS (TCOM), in 2018 and 2016, and IEEE WIRELESS COMMUNICATIONS LETTERS (WCL), in 2017 and 2014. He was also a recipient of the Post-Doctoral Research Award (PDRA) (first cycle) with the Qatar National Research Foundation (QNRF) in 2014, and the IEEE Richard E. Merwin Student Scholarship Award in July 2013.

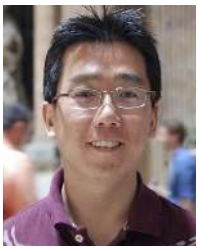

HEEJUNG YU (Senior Member, IEEE) received the B.S. degree in radio science and engineering from Korea University, Seoul, South Korea, in 1999, and the M.S. and Ph.D. degrees in electrical engineering from the Korea Advanced Institute of Science and Technology (KAIST), Daejeon, South Korea, in 2001 and 2011, respectively. From 2001 to 2012, he was with the Electronics and Telecommunications Research Institute (ETRI), Daejeon. From 2012 to 2019, he was with Yeungnam University, South Korea. He is currently an Associate Professor with the Department of Electronics and Information Engineering, Korea University, Sejong, South Korea. His research interests include statistical signal processing and communication theory.